Selective isolation of mono to quad layered 2D materials via sonication-based solution engineering

Tatsuya Nakamoto[1,2], Keigo Matsuyama[1,2], Takeshi Yoshimura[1], Norifumi Fujimura[1], and Daisuke Kiriya[1,2]*

[1] Department of Physics and Electronics, Osaka Metropolitan University
[2] Department of Basic Science, Graduate School of Arts and Sciences, The University of Tokyo

* kiriya@g.ecc.u-tokyo.ac.jp

Abstract

Mechanical exfoliation methods of two-dimensional materials have been an essential process for advanced device and fundamental sciences. However, the exfoliation method usually generates various thick flakes, and a bunch of thick bulk flakes usually covers an entire substrate. Here, we developed a method to selectively isolate mono- to quadlayers of transition metal dichalcogenides (TMDCs) by sonication in organic solvents. The analysis reveals the importance of low interface energies between solvents and TMDCs, leading to effective removal of bulk flakes under sonication. Importantly, a monolayer adjacent to bulk flakes shows cleavage at the interface, and the monolayer can be selectively isolated on the substrate. This approach can extend to preparing a monolayer device with crowded 17 electrode fingers surrounding the monolayer and for the measurement of electrostatic device performance.

Introduction

Two-dimensional (2D) materials have attracted the attention of next-generation devices and emerging physics because of their ideal layered confined structures and small dangling bonds[1–10]. In particular, transition metal dichalcogenides (TMDCs; MX_2, M = Mo, W and X = S, Se, Te) have been studied extensively in the past decade due to their band gap even at a thickness of three atomic layers[1,3]. Advanced electronics downscaling to 1.5 nm gate-operation[11] and second harmonic[12] and piezoelectric[13,14] behaviours by inversion symmetry breaking and exotic optoelectronic characters from moiré superlattices[15–17] have been developed, creating emerging electronics and physics. These

surpassing developments are generated in thin layers, usually up to quadlayers[15].

Various procedures for 2D material preparation have been developed; however, the process of preparing high-quality thin layers remains challenging, and the selective isolation of mono to quadlayers is difficult. Gas-phase growth methods, such as chemical[18,19] and physical vapour deposition processes[20,21], are promising for monolayer preparation; however, selective isolation of bi- to quadlayers remains challenging. Furthermore, these gas-phase methods include defective sites of transition metals and chalcogen atoms in the grown samples[22,23]. In the mechanical exfoliation method using scotch tapes, mono- to quadlayers with good crystallinity can be easily obtained. However, a large number of thick bulk flakes with a thickness of 10 nm or more are transferred simultaneously on the exfoliated substrates. The further worse situation is that the thin target layers are usually surrounded by or in contact with a vast number of bulk flakes; the situation essentially prevents from preparing well-designed devices on the thin layered TMDCs. In addition, once the flakes are placed on the substrates via the mechanical exfoliation process, the strong van der Waals interaction of the undesired bulk flakes on the substrates makes their selective removal difficult. Although dry transfer techniques via adhesives of polymers to selectively transfer a thin layer have succeeded in isolating identical layers[24,25], the process applies the flakes one by one, and much worse, insoluble residues from the polymer adhesives remains on the surface of the target material[26,27].

In this study, we developed a method to selectively isolate mono- to quad-layered TMDCs (i.e. MoS_2, WS_2 and WSe_2) on a usual Si/SiO_2 substrate by simply applying sonication in certain types of organic solvents. The selection of the solvent was critical for effectively removing the bulk flakes. The analysis indicates that ethanol and acetone exhibit low interface energy for TMDCs, and eventually, these solvents penetrate into the voids of the bulk flakes and lead to removal from the substrate. This effect is facilitated under sonication conditions. Importantly, this method enables the isolation of thin layers even adjacent to bulk flakes, cleaves the adjacent bulk flakes and extracts them from the substrate. As a demonstration, a device with an isolated monolayer MoS_2 flake was prepared with 17 electrodes arranged around the entire monolayer.

Results

Figure 1a represents the illustrative images of the sonication-based isolation process and the result of isolated thin layers on a substrate. The flakes were originally obtained by a usual mechanical exfoliation process[28], which includes a small number of thin layers, and simultaneously, a large number of bulk flakes (thicker than 10 nm) were

dominantly transferred on the Si/SiO_2 substrate. The exfoliated flakes were immersed in 5 ml of a solvent (water, acetonitrile, hexane, ethanol or acetone) and then sonicated at 64 W and 45 kHz for 5 min. The temperature of the solvent was monitored during sonication, which was constantly approximately 27 °C, changing only a few degrees even in harsh conditions. Figures 1b and 1c show the microscopy images of the sonication-based isolation process in ethanol. Thick bulk flakes were removed via the process, and monolayers and thin flakes were retained on the substrate, demonstrating that this process is effective for the selective isolation of thin layers, including monolayers. Photoluminescence (PL) and Raman spectrum measurements indicate that before and after the sonication-based process, negligible modulation of the electronic state is observed (Fig. S1). As shown in Figure 1d, the removal of the bulk flake is highly dependent on the solvent, and the removal ratio is dramatically reduced in ultrapure water. Therefore, the result of bulk removal is non-trivial, even with the sonication process, and the residual rate of bulk flakes is dependent on the solvent in the sonication-based process.

To examine bulk removability under the sonication-based method, we evaluated the residual bulk areas in various solvents before and after sonication by binarising the optical microscopy images (Fig. S2, S3 and S4). Figure 2a shows the residual area with sonication time under various solvents. Each solvent shows a significant difference in residual areas, and the deviation of residual areas between 1 and 5 min is smaller than the difference between solvents, revealing that this method is highly solvent dependent. Although the effect of cavitation generated during sonication is expected to increase with time, the slight variation in the application time implies that the solvent choice is the most crucial factor for bulk removability. A previous study has extensively reported the preparation of nano-inks by the dispersion of 1D or 2D materials through sonication, in which reducing the interaction between each material is the essence of making ink; the surface energy between the 2D materials and the solvents is essential for the dispersibility[29–32]. Thus, the affinity between TMDC and the solvent appears to be a major factor in determining bulk flake removal.

For further analysis, we considered the affinity between the TMDCs and solvents by parameters evaluated by the surface tension at the interface between a solid and a liquid [29,32]. The interfacial tension of solids and liquids is represented by Equation (1), which is divided into dispersive and polar components for the solids and liquids proposed by the Owen, Wendt, Rabel and Kaelble method[29];

$$\sigma_{\mathrm{sl}} = \sigma_{\mathrm{s}} + \sigma_{\mathrm{l}} - 2\left(\sqrt{\sigma_{\mathrm{s}}^{\mathrm{d}} \cdot \sigma_{\mathrm{l}}^{\mathrm{d}}} + \sqrt{\sigma_{\mathrm{s}}^{\mathrm{p}} \cdot \sigma_{\mathrm{l}}^{\mathrm{p}}}\right)$$

$$= \sigma_s^d + \sigma_s^p + \sigma_l^d + \sigma_l^p - 2\left(\sqrt{\sigma_s^d \cdot \sigma_l^d} + \sqrt{\sigma_s^p \cdot \sigma_l^p}\right) \quad (1)$$

where the lower letters of s and l represent the solid and liquid components, and the upper letters d and p represent the dispersion and polar components, respectively. By further modifying Equation (1), the interfacial tension σ_{sl} can be described by Equation (2). In Equation (2), the ratio of the polar and dispersive components of the solid and liquid describes the surface tension. The dispersive component is caused by the instantaneous dipole created by the fluctuation of charges due to the vibration of the molecules. The polar component is the amount of permanent dipole derived from the structure of polar molecules.

$$\sigma_{sl} = (\sqrt{\sigma_s^d}\sqrt{\frac{\sigma_s^p}{\sigma_s^d} + 1} - \sqrt{\sigma_l^d}\sqrt{\frac{\sigma_l^p}{\sigma_l^d} + 1})^2 + 2\sqrt{\sigma_s^d \sigma_l^d}$$

$$(\sqrt{\frac{\sigma_s^p}{\sigma_s^d} + 1}\sqrt{\frac{\sigma_l^p}{\sigma_l^d} + 1} - \sqrt{\frac{\sigma_l^p \sigma_s^p}{\sigma_l^d \sigma_s^d}} - 1) \quad (2)$$

According to Equation (2), the surface tension at the interface is potentially minimised when the polarity and dispersion component ratios of the solids and liquids show similar values[29]. Hence, the affinity of TMDCs and the solvent is maximised when the polar/dispersion component ratios have similar values. The component ratios are listed in Table S1. Each TMDC shows similar values for the component ratio evaluated from contact angle measurements. Figure 2b shows the residual area of the bulk flakes of each TMDC (MoS_2, WS_2 and WSe_2) regarding the difference in polar/dispersion component ratios for each solvent. In the case of solvents with high affinity to TMDCs, the difference in the polarity/dispersion ratios is small (close to 0), and the removability of the exfoliated bulk flakes is evident. We further evaluated the residual area of the bulk flakes in the mixture of water/acetone and water/ethanol (ethanol or acetone: 0%, 10%, 30%, 50% and 100%), which can modulate the surface tension, and monitored the identical region of interest on the substrates, as shown in Figures 2d and 2e. In both solvents, no significant change was observed up to the 50% mixture, whereas all bulk flakes were removed at 100%. Therefore, the sonication-based method has a threshold surface tension value for bulk removal.

In ethanol, which has a high affinity to TMDCs, we observed the lateral

rearrangement of bulk flakes on the Si/SiO_2 substrate without sonication. Immersion in ethanol for 72 h at 100 °C showed that some of the bulk flakes migrated or inverted on the substrate (Fig. 3). The results suggest that ethanol molecules penetrate the interface between the bulk flakes and the substrate. In contrast, when the solvent was water, which has a low affinity (Fig. 2b), no significant movements of the bulk flakes were observed. (Fig. S5). These results indicate the potential penetration of the solvent molecules into the substrate interface when the molecule has a high affinity to TMDCs. The cavitation under the sonication process facilitates bulk flake lift-up into the solvent. The floating bulk flakes were observed in the solvent only when sonication was applied, which was monitored through a visible Tyndall effect; the light was dispersed by the floating fragments in the solvent (Figs. S6a, S6b, and Movie 1). By drop casting the sonicated solvent, we observed flakes exceeding 100 μm (Fig. S6c). Therefore, the dispersed bulk flakes in the solvent were relatively large after the sonication-based process, not like dispersing fragments by collapsing into tiny nanopieces.

Figure 4a shows an atomic force microscopy (AFM) image of the backside of the balk flake. The bulk flake was first transferred on a substrate, peeled off from the substrate using an adhesion tape and flipped to observe the backside (Fig. S7). The AFM image shows that the bulk flakes have steps at the edge on the backside (Figs. 4a and 4b). This finding suggests that bulk flakes have voids at the interface with the Si/SiO_2 substrate; as a result, the solvent penetrates into the interface. In particular, this penetration of the solvent is critical under sonication. In contrast, thin layers, especially monolayers, have no voids; therefore, solvent penetration is less probable. Consequently, the bulk flakes lift up and rupture at the interface, with thin layers remaining on the substrate (Fig. 4c).

Most of the thin layers (monolayers, bilayers, etc.) are usually observed adjacent to bulk flakes by the mechanical exfoliation process, as shown in Figures 5a and 5b. The bulk flakes should be selectively removed from the substrates to isolate the thin layers. To achieve this isolation, the area of the thin layer should be adhered to on the substrate after the sonication-based process. For example, the sonication-based process shows the removal of the monolayer, which is adjacent to the bulk region (Fig. 5a). In contrast, in Figure 5b, the monolayer was kept adhesion to the substrate, and the bulk region was selectively removed by rupturing at the boundary to the monolayer. These results suggest that the area of thin layers and the boundary at the thin/thick layers decide the retention of thin layers on substrates after the sonication-based process.

We evaluated the rupture force and adhesion strength of monolayer MoS_2 to understand the sonication-based isolation process. Table 1 shows the mechanical

properties of the monolayer MoS_2; the adhesion strength of MoS_2 was evaluated in a previous study[33] with a force–distance curve for MoS_2-MoS_2 separation (30.1 MPa) and is approximately greater than that of MoS_2-SiO_2 (see Supplementary Information)[34]. This deviation shows no considerably large change in the estimation for the following hypothesis; therefore, we applied this force as the adhesion. In the case of monolayers (thickness ~0.7 nm), the adhesion force to SiO_2 should be larger than the rupture force (30 MPa) at the boundary of the bulk region to isolate and separate them from the adjacent bulk region[35]. According to this hypothesis and the parameters shown in Table 1, Equations (3) and (4) are obtained for the delamination condition of the bulk region and the simultaneous isolation of the monolayer by rupturing at the boundary:

$$30.1 \times S > 30 \times 0.7 \times L \quad (3)$$

$$S/L > 0.70 \quad (4)$$

where S is the area of the thin layer (μm^2), and L is the boundary at the interface between the thin layer and the bulk region (μm).

Equation (4) suggests that when the ratio of the thin layer area is larger than a certain length of the boundary, $S/L > 0.70$, the delamination from the substrate is interrupted, and the thin layers remain. Given that Equation (4) is assumed for a monolayer to remain, the rupture strength for the flakes thicker than the bilayers should be larger and the S/L should be more than 0.70. Figure 5c shows the residual area of thin layers (mono- to pentalayers) to the relationship with S/L. According to the experimental results, bi- and over trilayers were also retained with Equation (4), although some regions were deficient along with the sonication-based process. These observations are consistent with the results showing that the sonication-based process maintains the large size of the delaminated bulk flakes after the sonication-based process (Fig. S6c).

For the isolated monolayers, we applied the sonication-based process for a long time and revealed that the monolayer was gradually removed from the edges of the flake (Fig. S8). Therefore, the monolayer flake was not peeled off at once via the sonication-based process. This finding is because even if a partial area at the edge is delaminated from the substrate, the area S in Equation (4) is large enough, and the monolayer then ruptures at the delaminated boundary. According to the above-mentioned results, the isolation process can be summarised as follows: i) the solvent penetrates through the voids, and the perturbation of sonication causes the region to detach from the substrate, especially for the thick bulk region; and ii) the detachment of the thin region is less likely

to occur because of the tendency of rupture inside the thin region, and the retained thin region is isolated on the substrate (Fig. 4b).

By removing a large number of bulk flakes around the monolayer flakes and by achieving isolation, a bunch of electrodes surrounding the entire monolayer flake can be accessed. This situation is completely different from the situation surrounding various thick layers, which prevents accessing electrodes through the disconnection of the electrical path. Figures 6 and S9 show a monolayer device with 17 metal lines accessed from 360 ° directions. Electrical property was evaluated for the three hall bar devices on the monolayer. Each device shows the gate dependency under the gate voltage (V_G) applying 0 V to 30 V. The longitudinal resistance R_{xx} showed gate dependency, the value ranged 33–56 MΩ at a gate voltage of 30 V. The high resistance would include some residual resistance at the contact resistance. In another device with a trilayer flake with 7 fingered device, as shown in Figure S10, showed a gate dependency with the longitudinal resistance R_{xx} = 108–119 kΩ at V_G = 30 V. The resistance is relatively small and the estimated contact resistance is ~100 kΩ. These issues on the high contact resistance are still in challenge to realise 2D electronics[36–39].

Discussion

In conclusion, we presented a general method capable of isolating mono- to quadlayers selectively on Si/SiO_2 substrates by applying the sonication-based method. In this method, the exfoliated bulk flakes are selectively removed under solvents in a condition of minimised surface tension. The voids at the backside of the bulk flakes are responsible for the removal of the bulk flakes. The area (S) of the thin-layer region and the boundary (L) between the thin and thick regions are essential for the isolation of the thin layers on the substrate, and the $S/L > 0.70$ is estimated as the threshold to isolate monolayers. This isolation method via the sonication-based process is applicable to various TMDCs, including MoS_2, WS_2 and WSe_2. Preparing an isolated monolayer MoS_2 flake can be applied to three hall bar devices, including 17 electrodes placed around the monolayer. Our developed method paves the way for engineering of 2D materials, impacting the development of 2D nanoelectronics and physics.

Methods

Sample preparation. MX_2 was prepared by the mechanical exfoliation method on a 260

nm thermal oxide covered silicon substrate (Silicone Valley Microelectronics INC.). The substrate with the tape was left under a vacuum condition of approximately 100 Torr for 24–48 h at room temperature. The substrate was then immersed in a solvent (water (Milli-Q), acetonitrile (Sigma-Aldrich or Tokyo Chemical Industry), hexane (FUJIFILM Wako Pure Chemical), ethanol (Kishida Chemical) or acetone (Kishida Chemical)), and sonication was applied (45 kHz, 64 W) by a bath sonicator (CREST ULTRASONICS Co., CP230D). The solvent was removed by N_2 blow after sonication. A PL Raman spectrometer (HORIBA Scientific, 532 nm excitation with ~2.7 W cm^{-2}) was used to identify the monolayer and to observe the electronic state and strain change before and after sonication. HF for etching SiO_2 in Figure S7 was purchased from Wako Pure Chemical to obtain the back side MoS_2, which was observed with atomic force microscopy (SII instruments) in Figure 4b.

Device fabrication and measurements. The electrode patterns were drawn by electron beam lithography (ELS-7500, ELIONIX). Au (100 nm)/Ti (5 nm) films were deposited using an electron beam evaporator. The patterns were obtained by a lift-off process in 2-butanone (FUJIFILM Wako Pure Chemical). Before the measurements, the devices were annealed at 100 °C on a hotplate. The measurements were done with a semiconductor parameter analyser (Keysight, B-1500A). Each device shown in Figure 6 was measured by applying the gate voltage from 0 V to 30 V, with an excitation current of 50 pA.

Acknowledgements

We thank K. Miyaji and Y. Igarashi for advice on the analysis of removability of bulk flakes. Materials preparation and characterization were funded by JST FOREST Program, Grant Number JPMJFR2125. Device fabrication and characterization were funded by JSPS KAKENHI (20H02574).

References

1. Lien, D.-H. *et al.* Large-area and bright pulsed electroluminescence in monolayer semiconductors. *Nat. Commun.* **9,** 1229 (2018).
2. Jariwala, D., Sangwan, V. K., Lauhon, L. J., Marks, T. J. & Hersam, M. C. Emerging device applications for semiconducting two-dimensional transition metal dichalcogenides. *ACS Nano* **8,** 1102–1120 (2014).
3. Splendiani, A. *et al.* Emerging photoluminescence in monolayer MoS_2. *Nano Lett.* **10,** 1271–1275 (2010).
4. Chhowalla, M. *et al.* The chemistry of two-dimensional layered transition metal dichalcogenide nanosheets. *Nat. Chem.* **5,** 263–275 (2013).
5. Zeng, M., Xiao, Y., Liu, J., Yang, K. & Fu, L. Exploring two-dimensional materials toward the next-generation circuits: From monomer design to assembly control. *Chem. Rev.* **118,** 6236–6296 (2018).
6. Bhimanapati, G. R. *et al.* Recent advances in two-dimensional materials beyond graphene. *ACS Nano* **9,** 11509–11539 (2015).
7. Kuc, A., Zibouche, N. & Heine, T. Influence of quantum confinement on the electronic structure of the transition metal sulfide TS_2. *Phys. Rev. B* **83,** 245213 (2011).
8. Mak, K. F., Lee, C., Hone, J., Shan, J. & Heinz, T. F. Atomically thin MoS_2: A New direct-gap semiconductor. *Phys. Rev. Lett.* **105,** 136805 (2010).
9. Man, M. K. L. *et al.* Protecting the properties of monolayer MoS_2 on silicon based substrates with an atomically thin buffer. *Sci. Rep.* **6,** 20890 (2016).
10. Schneider, C., Glazov, M. M., Korn, T., Höfling, S. & Urbaszek, B. Two-dimensional semiconductors in the regime of strong light-matter coupling. *Nat. Commun.* **9,** 2695 (2018).
11. Desai, S. B. *et al.* MoS_2 transistors with 1-nanometer gate lengths. *Science* **354,** 99–102 (2016).
12. Li, Y. *et al.* Probing symmetry properties of few-layer MoS_2 and h-BN by optical second-harmonic generation. *Nano Lett.* **13,** 3329–3333 (2013).
13. Duerloo, K.-A. N., Ong, M. T. & Reed, E. J. Intrinsic piezoelectricity in two-dimensional materials. *J. Phys. Chem. Lett.* **3,** 2871–2876 (2012).

14. Cui, C., Xue, F., Hu, W.-J. & Li, L.-J. Two-dimensional materials with piezoelectric and ferroelectric functionalities. *NPJ 2D Mater. Appl.* **2,** 18 (2018).
15. Wu, Z. *et al.* Even–odd layer-dependent magnetotransport of high-mobility Q-valley electrons in transition metal disulfides. *Nat. Commun.* **7,** 12955 (2016).
16. Miao, S. *et al.* Strong interaction between interlayer excitons and correlated electrons in WSe_2/WS_2 moiré superlattice. *Nat. Commun.* **12,** 3608 (2021).
17. Xie, L. *et al.* WS_2 moiré superlattices derived from mechanical flexibility for hydrogen evolution reaction. *Nat. Commun.* **12,** 5070 (2021).
18. Ahn, J.-H., Parkin, W. M., Naylor, C. H., Johnson, A. T. C. & Drndić, M. Ambient effects on electrical characteristics of CVD-grown monolayer MoS_2 field-effect transistors. *Sci. Rep.* **7,** 4075 (2017).
19. Lee, Y.-H. *et al.* Synthesis of large-area MoS_2 atomic layers with chemical vapor deposition. *Adv. Mater.* **24,** 2320–2325 (2012).
20. Ono, R. *et al.* Elucidation of PVD MoS_2 film formation process and its structure focusing on sub-monolayer region. *Jpn. J. Appl. Phys.* **61,** SC1023 (2022).
21. Wu, S. *et al.* Vapor–solid growth of high optical quality MoS_2 Monolayers with near-unity valley polarization. *ACS Nano* **7,** 2768–2772 (2013).
22. Hong, J. *et al.* Exploring atomic defects in molybdenum disulphide monolayers. *Nat. Commun.* **6,** 6293 (2015).
23. Zhou, W. *et al.* Intrinsic structural defects in monolayer molybdenum disulfide. *Nano Lett.* **13,** 2615–2622 (2013).
24. Kinoshita, K. *et al.* Dry release transfer of graphene and few-layer h-BN by utilizing thermoplasticity of polypropylene carbonate. *NPJ 2D Mater. Appl.* **3,** 22 (2019).
25. Meitl, M. A. *et al.* Transfer printing by kinetic control of adhesion to an elastomeric stamp. *Nat. Mater.* **5,** 33–38 (2006).
26. Jain, A. *et al.* Minimizing residues and strain in 2D materials transferred from PDMS. *Nanotechnology* **29**, 265203 (2018).
27. Glasmästar, K., Gold, J., Andersson, A.-S., Sutherland, D. S. & Kasemo, B. Silicone transfer during microcontact printing. *Langmuir* **19,** 5475–5483 (2003).
28. Novoselov, K. S. *et al.* Electric field effect in atomically thin carbon films. *Science* **306**, 666–669 (2004).
29. Shen, J. *et al.* Liquid phase exfoliation of two-dimensional materials by directly probing and matching surface tension components. *Nano Lett.* **15,** 5449–5454 (2015).
30. Lotya, M., King, P. J., Khan, U., De, S. & Coleman, J. N. High-concentration,

surfactant-stabilized graphene dispersions. *ACS Nano* **4,** 3155–3162 (2010).
31. He, Z. & Alexandridis, P. Ionic liquid and nanoparticle hybrid systems: Emerging applications. *Adv. Colloid Interface Sci.* **244,** 54–70 (2017).
32. Wang, M. *et al.* Surface tension components ratio: An efficient parameter for direct liquid phase exfoliation. *ACS Appl. Mater. Interfaces* **9,** 9168–9175 (2017).
33. Rokni, H. & Lu, W. Direct measurements of interfacial adhesion in 2D materials and van der Waals heterostructures in ambient air. *Nat. Commun.* **11,** 5607 (2020).
34. Sanchez, D. A. *et al.* Mechanics of spontaneously formed nanoblisters trapped by transferred 2D crystals. *Proc. Natl. Acad. Sci.* **115,** 7884–7889 (2018).
35. Bertolazzi, S., Brivio, J. & Kis, A. stretching and breaking of ultrathin MoS_2. *ACS Nano* **5,** 9703–9709 (2011).
36. Shen, P.-C. *et al.* Ultralow contact resistance between semimetal and monolayer semiconductors. *Nature* **593,** 211–217 (2021).
37. Houssa, M. *et al.* Contact reesistance at MoS_2 -based 2D metal/semiconductor lateral heterojunctions. *ACS Appl. Nano Mater.* **2,** 760–766 (2019).
38. Liu, W. *et al.* High-performance few-layer-MoS_2 field-effect-transistor with record low contact-resistance. *Electron Devices Meet. IEDM 2013 IEEE Int.* 19.4.1-19.4.4 (2013).
39. Zhong, H. *et al.* Interfacial properties of monolayer and bilayer MoS_2 contacts with metals: Beyond the energy band calculations. *Sci. Rep.* **6,** 21786 (2016).
40. Li, P. *et al.* In situ nanomechanical characterization of multi-layer MoS_2 membranes: From intraplanar to interplanar fracture. *Nanoscale* **9,** 9119–9128 (2017).

Figure caption

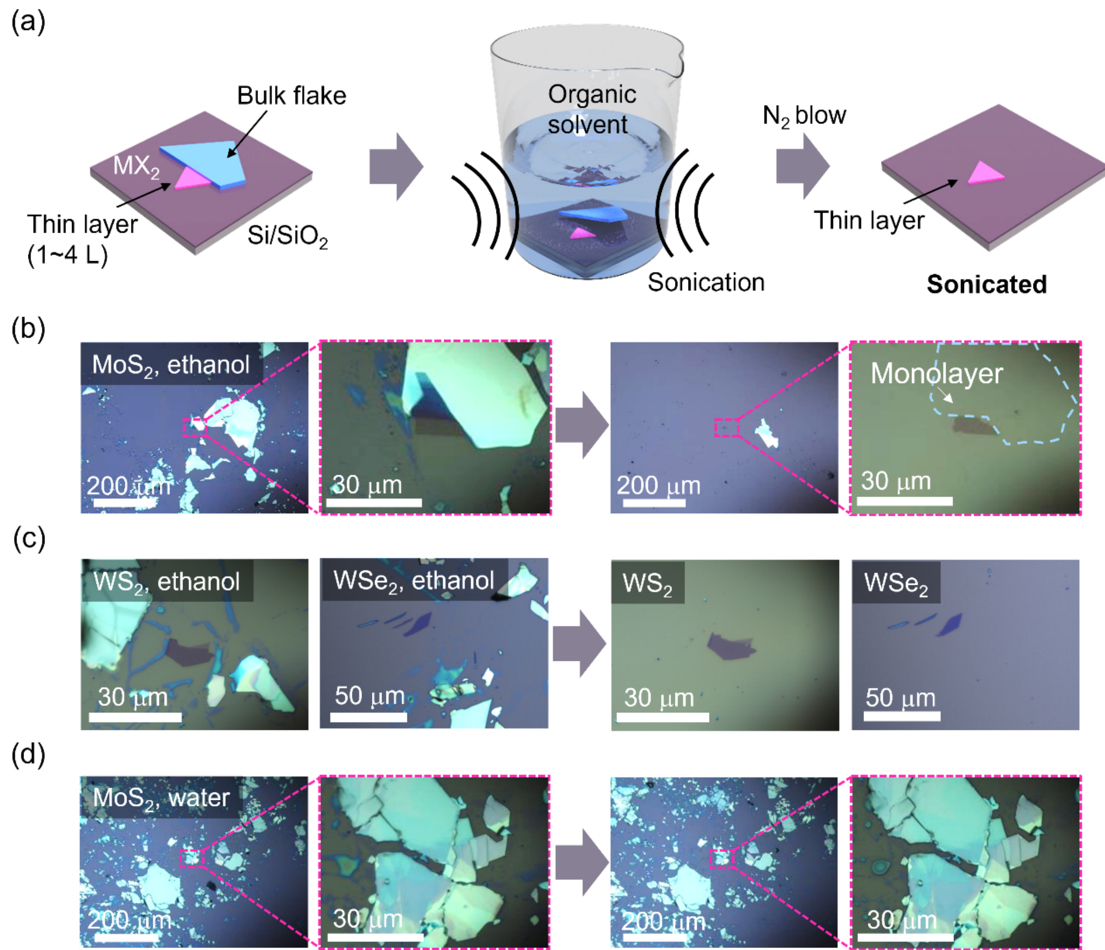

Figure 1. Isolation of the exfoliated MX_2 thin layers (mono- to quadlayers) via the sonication-based solution process. (a) Schematic of the sonication-based process for removing adjacent bulk flakes and isolating a thin layer. (b–d) Optical microscopy images of the as-exfoliated (left) and sonicated (right) samples on the substrate. (b) Monolayer MoS_2 adjacent to bulk flakes and the isolation of the monolayer by sonication in ethanol. The dashed lines represent the location of the bulk region before the process. (c) Isolation of WS_2 and WSe_2 thin layers before and after the sonication process in ethanol. (d) MoS_2 bulk flakes before and after the sonication process in ultrapure water.

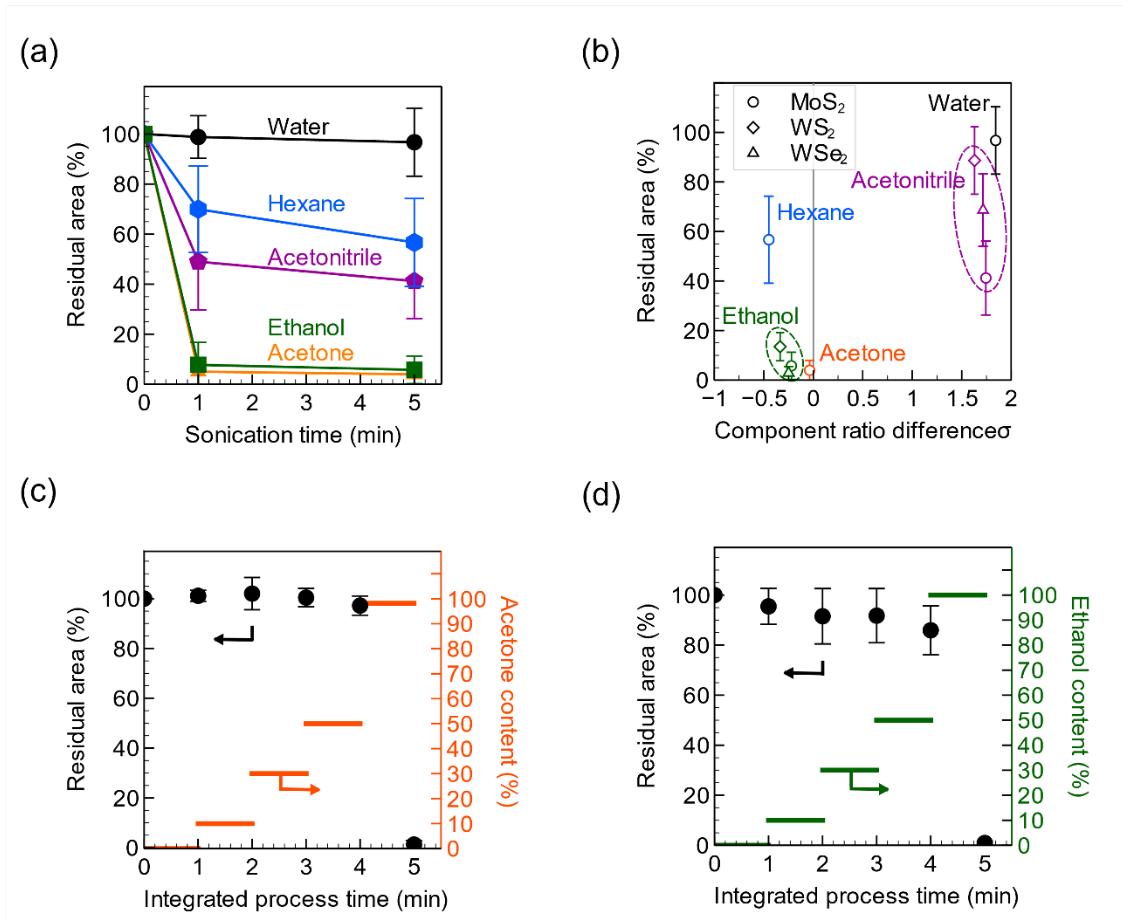

Figure 2. Solvent dependence of bulk removability. (a) Residual areas of MoS_2 bulk flakes on the substrate after sonication for 1 and 5 min in each solvent (water, hexane, acetonitrile, ethanol and acetone). The area of the bulk flakes on the unprocessed original substrate was defined as 100%, and the residual area after the process was calculated. (b) Bulk residuals for different polar dispersion component ratios of various solvents for MX_2 (MoS_2, WS_2 and WSe_2). The grey lines indicate the case with no difference in component ratios; the farther away from the line, the lower the affinity between MX_2 and solvents. (c and d) The residual bulk area for the identical location on substrates along with gradually changing solvents from ultrapure water to acetone (c) or ethanol (d). The black plots represent the areal ratio of bulk residuals, and the orange (c) or green (d) lines represent the concentration of acetone (c) or ethanol (d) added to ultrapure water to prepare a specific concentration (0%, 10%, 30%, 50% and 100%).

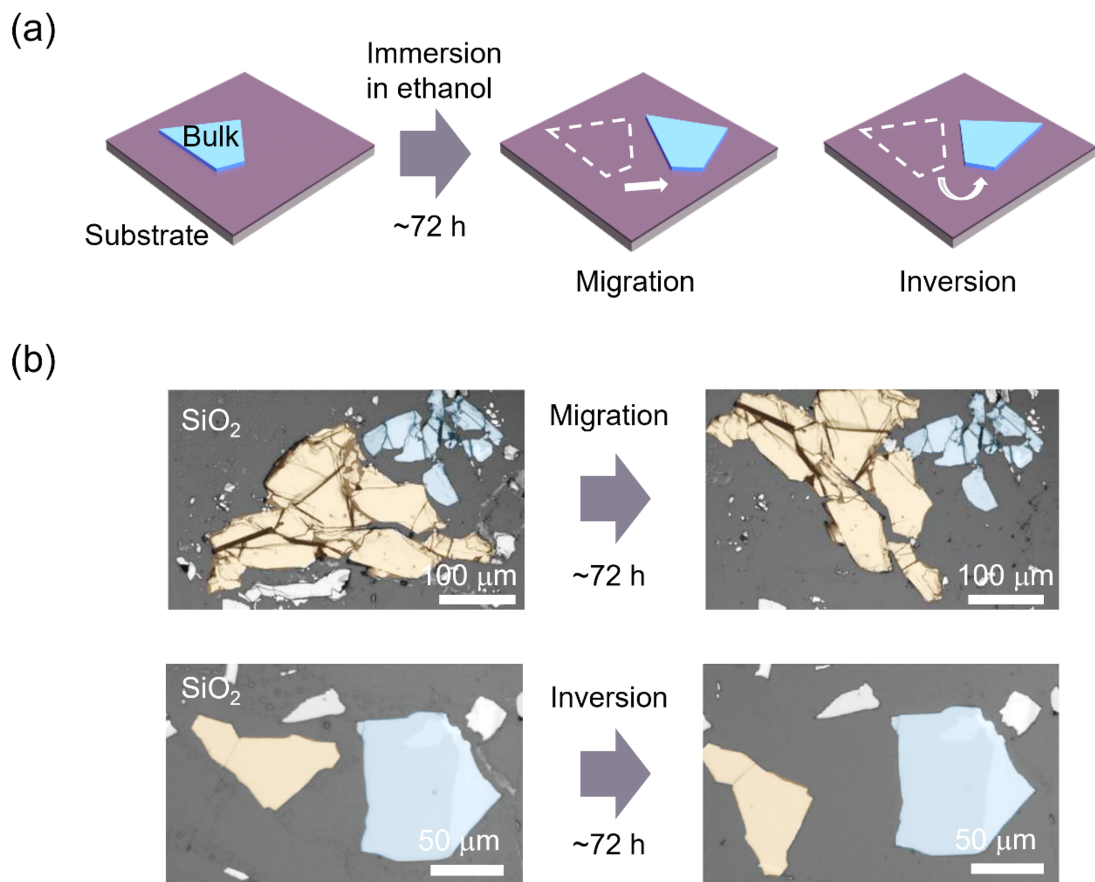

Figure 3. Immersion of the substrate with exfoliated MoS_2 into ethanol. (a) Schematic of in-plane migration and inversion of bulk flakes on the substrate by immersion in ethanol. (b) Optical microscopy images of the migration (top) and inversion (bottom) of bulk flakes on the substrate by immersion in ethanol for 72 h at 100 °C. The left images were obtained after exfoliation, and the right images were obtained after immersion. The pseudo colours yellow and blue are used to clearly identify the relative positions.

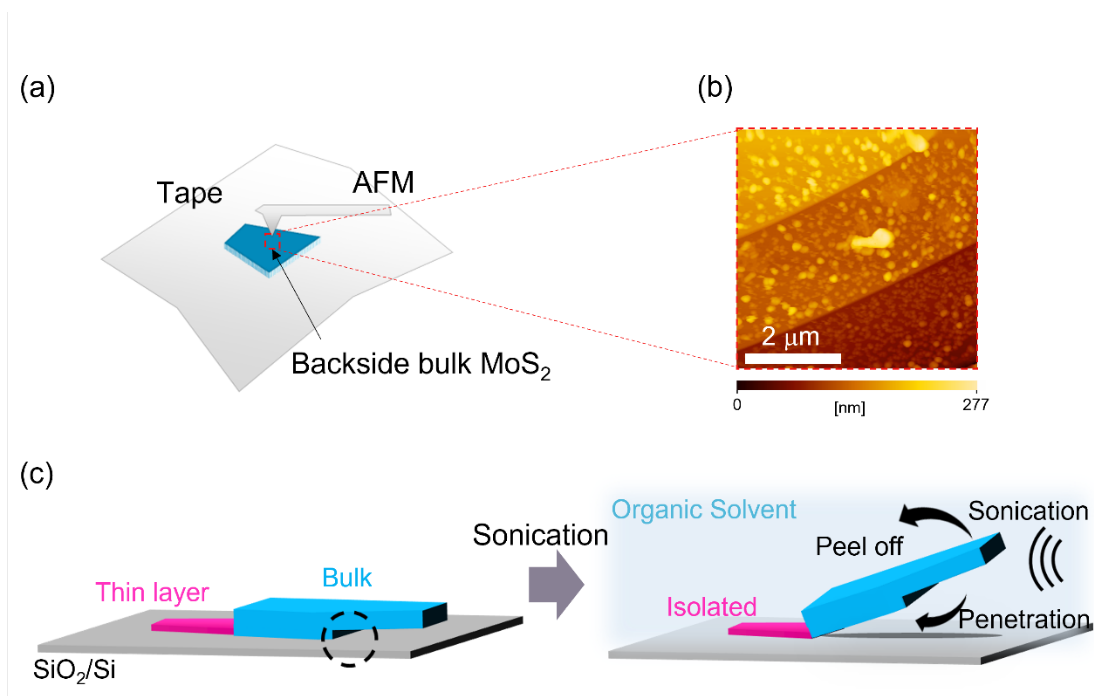

Figure 4. Mechanism of bulk removal from the substrate. (a) Schematic of the observation of the backside of the bulk flake. (b) AFM image of the backside of the bulk flake. (c) Schematic of the bulk removal and isolation of a thin layer under the sonication process.

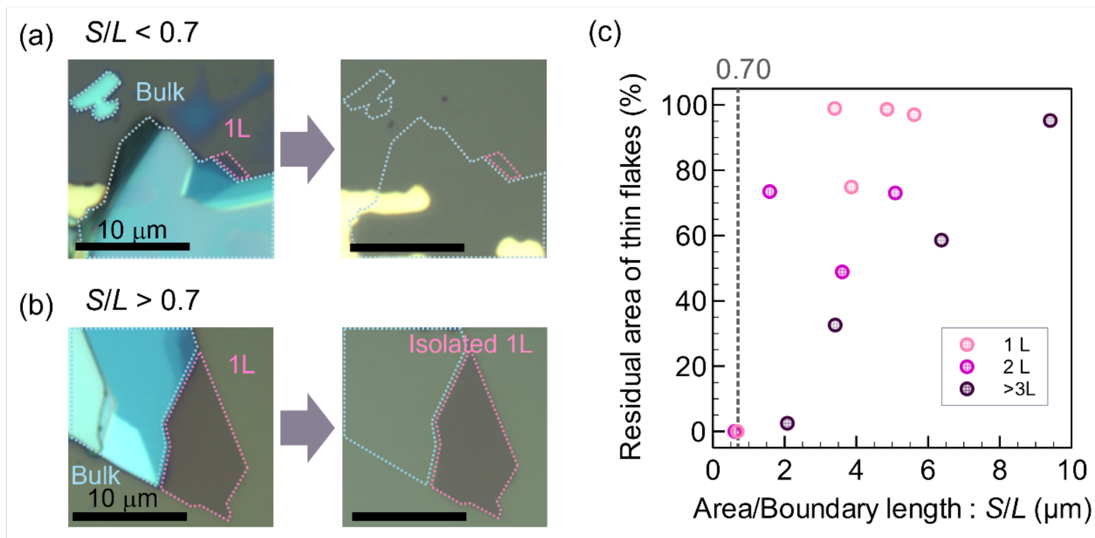

Figure 5. Mechanistic insight into the remaining monolayer via the sonication-based process. (a and b) Monolayer flakes adjacent to the bulk flake at $S/L < 0.7$ (a) and $S/L > 0.7$. (b) The left and right images show the as-exfoliated sample and the sample after the sonication process, respectively. The gold region in Figure 5a is the identification marker on the substrate. (c) S/L dependence of the residual area of thin layers (mono- to pentalayers) after the ethanol sonication process. Samples are categorised as monolayers (1L: pale orange), bilayers (2L: purple) and thin flakes (>3L: grey). The dashed lines represent the criteria of the monolayer removal obtained from the parameters shown in Table 1, which corresponds to $S/L = 0.70$.

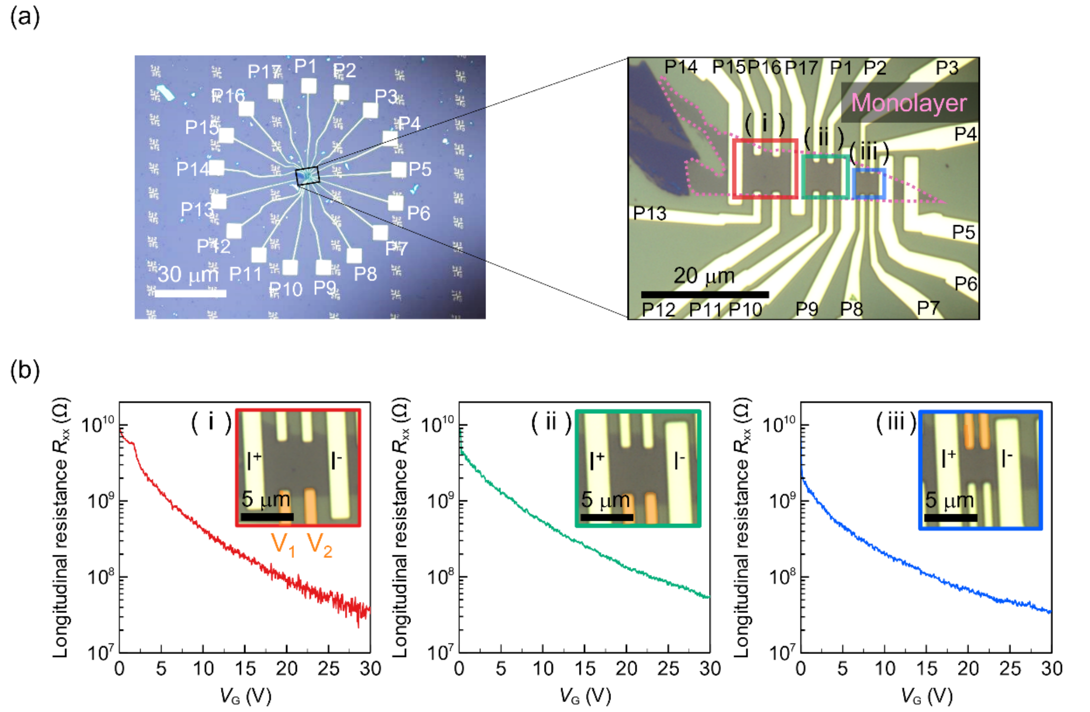

Figure 6. Demonstration of a multiple electrode-connected device for an isolated monolayer. (a) Overview of the optical microscopy image of the device. P1 to P17 indicate that the electrodes connect to the monolayer. The right image shows the magnified image of the device. Three hall bar structures are fabricated on the monolayer. (b) Gate dependence of the longitudinal resistance R_{xx} for the three devices shown in Figure 6a. Each graph (i, ii and iii) corresponds to the devices in red (i), green (ii) and blue (iii) boxes in Figure 6a.

Table 1. Rupture and adhesion strength of monolayer MoS_2

	Thickness of the Sample (nm)	Pressure	Force (μN)
Rupture strength	0.7	30 GPa [1]	$21 \times L$ [1]
	0.7	39 GPa [2]	$28 \times L$ [2]
Adhesion strength	–	30.1 MPa [3]	$30 \times S$ [3]

Note: L is defined as the length (μm) of the boundary between the monolayer and the accompanying bulk region. S is defined as the in-plane area (μm^2) of the monolayer. [1] is measured by breaking the exfoliated monolayer with an atomic force microscope probe in reference [35]; [2] is calculated using molecular dynamics simulations in reference [40]; [3] is calculated from the force–displacement curve during the delamination process between MoS_2-MoS_2 layers in reference [33].